Tunable Magnetically Actuated Retraction Device for Improved Control During Endoscopic Tissue Manipulation

Haley Mayer, Eran Shlomovitz, James Drake, Thomas Looi, *Member, IEEE*, and Eric Diller, *Senior Member, IEEE*

***Abstract*— *Objective*: Endoscopic submucosal dissection (ESD) is a minimally-invasive method for removing gastrointestinal lesions. Adoption has been slow due to the procedure's technical difficulty, length of surgery, and lack of appropriate tools. Tissue traction is required to reduce the technical difficulty of ESD and ensure safe lesion removal. This paper presents the first ESD retraction device that is wireless, endoscope-independent, and provides adjustable traction force control. *Methods*: The magnetic retraction device is 3.25 mm wide and 45 mm long. It is actuated wirelessly by a rotating permanent magnet held outside the abdomen. The device design is informed by a presented model of actuation, and we show characterization of the device actuation, validation of mechanical retraction, and clinical feasibility through an ex-vivo experiment. *Results*: Experiments show that the device retracts 20 mm at 0.2 millimeters per second and generates a peak retraction force of 7.98 N and a four-peak average of 5.62 N at an external magnet-to-device distance of 55 mm. Ex-vivo testing with a gastric porcine model was performed with a dissection speed of 11.3 square centimeters per hour, 1.25 times faster than the reported international benchmark. *Conclusion*: This enhanced tissue control would greatly improve patient clinical outcomes by expanding the use of ESD, shortening procedure times, minimizing complications, and potentially further expand its future medical applications. *Significance*: This work grants surgeons improved tissue control throughout an ESD procedure, providing adequate visualization of the dissection plane, control independent of the flexible endoscope, and deployment anywhere along the gastrointestinal tract.**

***Index Terms*— Endoscopic submucosal dissection, flexible endoscopy, gastroenterology, magnetic actuation, medical robotics, micro-transmission, tissue retraction, twisted string actuator.**

I. Introduction

GASTROINTESTINAL (GI) malignancy is a major cause of death and disability worldwide, represents the most frequent type of cancer diagnosis and death, and imposes a major healthcare burden [1]. If detected early, pre-malignant lesions or superficial malignancies that do not invade the muscle layer of the GI tract can ideally be detected and removed without the need for major surgery of the affected organ, ensuring organ preservation [2], [3]. In this case, endoscopic mucosal resection is a piecemeal approach used to surgically remove the lesion in multiple small sections using snares. Compared to en bloc resection, this approach is associated with a higher rate of local re-occurrence because the tools used are limited to removing only small fragments, increasing the likelihood of leaving behind residual tissue [4], [5]. While an endoscopic approach to precancerous lesion resection can avoid the need for major surgery, it is difficult to perform en bloc resection for lesions larger than 20 mm using standard polypectomy or endoscopic mucosal resection techniques [6].

Endoscopic submucosal dissection (ESD) is one of the primary flexible-endoscopic techniques for minimally invasive, organ preserving endoscopic resections. ESD is used to remove lesions in one solid piece from the GI tract, making it an effective way to treat early stage cancer and precancerous lesions, often leading to an excellent prognosis. The ESD technique involves marking the cutting lines on the mucosa around the circumference of the lesion, lifting the tissue off the muscle wall via submucosal fluid injection, dissecting free the deep margin of the lesion, and then removing the lesion from the GI wall (as shown in Fig. 2). This difficult and relatively new procedure has been accepted as the standard treatment in some Asian countries due to favorable short- and long-term outcomes [7], such as higher en bloc resection rates, lower local re-occurrence rates, and higher endoscopic curability [8], [9]. Its adoption in Western countries, however, has been poor due to the technical difficulty of this procedure, length of surgery, and lack of appropriate tools available [10]. To ensure a safe removal with negative tissue margins, tissue tension is required to lift the lesion, separating the tissue layers, and providing visualization of the dissection plane [11].

Conventional retraction techniques developed by surgeons for ESD and endoscopic mucosal resection are unable to provide adequate control of tissue tension. As tissue is cut away, tension decreases resulting in loss of visualization and tissue layer separation, leading to procedural complications [12]. Difficulty in maintaining adequate visualization of the dissection plan during ESD is recognized as one of the greatest barriers to widespread adoption of ESD [13]. Thus, there is a need for a medical device that gives surgeons better independent control over tissue tension to reduce the technical difficulty of the ESD technique.

Various methods of applying traction have been developed, where the most-used method clinically being clipping a string onto the lesion. However, these tools have limitations in delivering continuous and dynamic traction throughout the procedure. For conventional cable-actuated tools deployed through a flexible endoscope, their performance at the distal end within a surgical workspace is highly dependent on the shape of the endoscope. In particular, the maximum sustained pull force drastically decreases when endoscopes are in retroflexion (needed to work in the colon and esophageal portions of the stomach) when compared to a linear configuration [14]. This is primarily due to increased internal friction within the endoscope's working channel which limits force transmission. There exist other partially-adopted tools for ESD that have been developed by surgeons to provide a degree of traction during the ESD technique. Some examples include the ProdiGI Traction Wire (Medtronic, Minneapolis, Minnesota, USA [15]), EndoTrac (TOP

This work was supported by CIHR Project Grant 452287 and the Hospital for Sick Children Foundation. (Corresponding author: Eric Diller.)

Haley Mayer is with the Department of Mechanical and Industrial Engineering, University of Toronto, Posluns Center for Image Guided Innovation and Therapeutic Intervention (PCIGITI) at the Hospital for Sick Children, and Robotics Institute, University of Toronto, Toronto, ON M5S 3G8, Canada.

Eran Shlomovitz is a general surgeon in diagnostic radiology with the University Health Network, Toronto, ON M5G 2C4, Canada.

Eric Diller is with the Department of Mechanical and Industrial Engineering, Robotics Institute, and the Institute for Biomedical Engineering, University of Toronto, Toronto, ON M5S 3G8, Canada (e-mail: eric.diller@utoronto.ca)

James Drake, and Thomas Looi are with the Wilfred and Joyce Posluns Center for Image Guided Innovation and Therapeutic Intervention (PCIGITI) at the Hospital for Sick Children, Toronto, ON M5G 1E8, Canada.

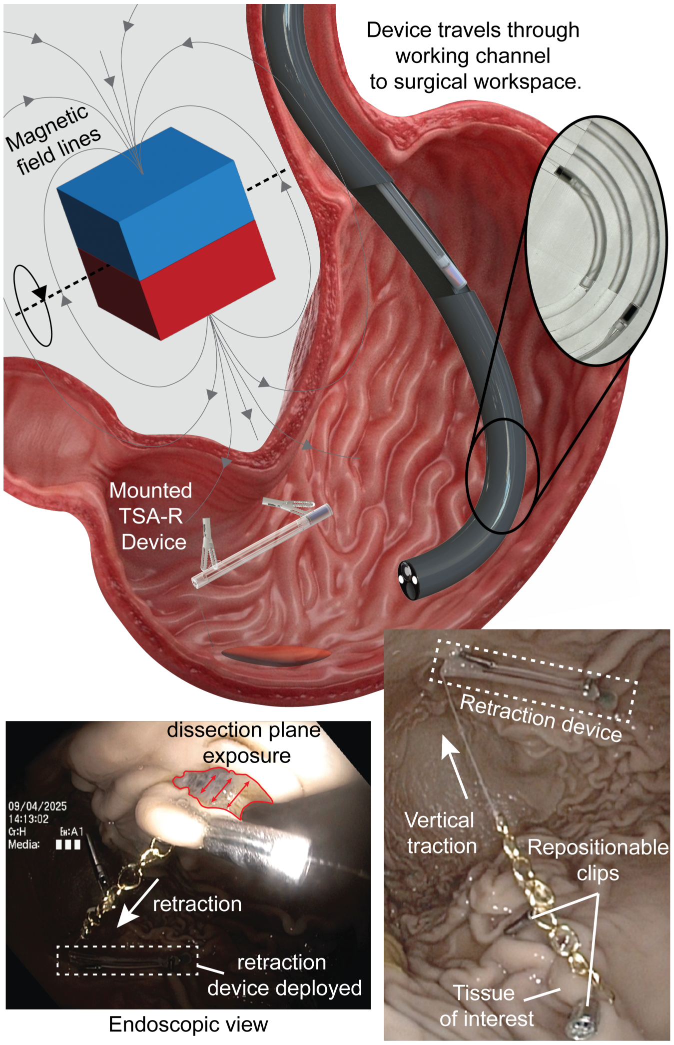

Fig. 1. Schematic of retraction device render controlled with magnetic actuation using a single permanent magnet. Exploded image shows device bending to pass through the working channel of the flexible endoscope. Endoscopic view (image enhanced by lightened shadows, reduced exposure, and increased brightness) from the flexible endoscopes point-of-view of tissue retraction using the device. Endoscopic view (image enhanced by lightened shadows, reduced exposure, and increased brightness) with components labeled. The mechanisms components are further detailed in Fig. 3.

Corporation, Tokyo, Japan [16]), S-O clip (ZEON Medical, Tokyo, Japan), and Multi Loop Traction Device (Boston Scientific Japan, Tokyo, Japan). These devices are initially anchored into the surgical workspace using single-use repositionable clips. In the case of the clip-string method traction is applied by pulling on the string that is brought out of the mouth or anus directly or via a pulley clip such that traction can be applied outside the body by the surgeon or surgical assistant [17]. These string approaches are crude and don't allow a precise or adjustable angle and tension to be applied. Other approaches use an elastic, spring, or chain of elastics in tandem with single-use repositionable clips to provide retraction by pulling opposite the lesion. The repositionable clips can be installed into the wall of the GI lumen to allow initial traction in any reachable direction. However they cannot provide adequate control of tissue tension. As tissue is cut away the distance between the anchor points decrease and this results in a decrease in tension due to the loss in elasticity. This can lead to loss of visualization and tissue layer separation, leading to procedural complications.

Robot-assisted endoscopy approaches aim to improve tissue control and manipulation by providing an additional arm within the surgical workspace via an endoscope. Specialized flexible endoscopes with multiple working channels or external attachments are used to add additional arms with varying degrees of freedom. Examples of current robotic research systems and their respective metrics include transendoscopic flexible parallel continuum robot [18] achieved a dissection speed of 65.37 cm^2/hour and procedural time of 22.45 min during a single in-vivo gastric porcine procedure; Flex Robotic System [19] achieved a dissection speed of 34.1 ± 19.14 cm^2/hour and procedural time of 5.53 ± 9.85 min during multiple (n=20) ex-vivo colon porcine procedures; MASTER [20] achieved a dissection speed of 24.2 ± 20 cm^2/hour and procedural time of 39 ± 14.8 min during multiple (n=5) in-vivo gastric porcine procedures; and STRAS [21] achieved a dissection speed of 38.7 ± 35 cm^2/hour and procedural time of 34.25 min during multiple (n=12) in-vivo colon porcine procedures. These endoscopic robotic-based systems are limited by their dependence on the GI endoscope; similar to conventional cable-actuated tools, their performance is dependent on the configuration of the endoscope. The strength of the add-on robotic arms are dependent on the stiffness, positioning, and orientation of the endoscope [14]. This force reduction is especially problematic for lesions located in difficult areas that require an endoscope to bend in retro-flexion. Furthermore, visualization for these add-on systems is coupled to the movement of the endoscope, resulting in periodic loss of the dissection plane during mucosal dissection.

Magnetic actuation is a viable alternative to the conventional cable-actuated approaches mentioned above. Low-frequency magnetic fields can safely penetrate through all biological tissues and non-metallic materials without damage or distortion, and can wirelessly actuate mechanisms onboard a device [22]. Existing magnetically-actuated retraction devices use either an anchor or a spooling technique. Magnetic anchor devices for ESD of large early gastric cancers endoscopically attach a small permanent magnet to the lesion and use a large electromagnet outside the body to manipulate the lesion [4], [23]. During in-vivo gastric ESD procedures (n=25) an average procedural time of 80 min and a dissection speed of 14.14 cm^2/hour was achieved using the magnetic anchor system [4]. Magnetic spooling retraction devices work by incorporating a magnetic gear to the existing magnetic anchor system to control the degree of retraction. Spooling devices retract tissues of interest by winding an internal actuating magnet that spools to collect the string. At a maximum actuation depth of 40 mm this system can only pull a 100 g weight [24]. While these systems can provide retraction in any desired direction, their external actuation units must be large and cumbersome in order to generate adequate force, and they are unable to work at an abdominal depth greater than 40 mm without losing magnetic coupling [23], [24].

Actuation of magnetic devices in the body at longer distances is challenging because the magnetic field generated by an external magnet will scale with one over distance cubed. This steep drop-off in field means that it is challenging to achieve pull forces required (up to 3 N are required to retract GI lesions). A magnetic field generator must be substantially large to generate sufficient force through direct pulling at the distance required from the abdominal wall to the point of intervention, which can be up to 170 mm [25]. To augment the output of magnetically-actuated devices, micro-transmissions like gearbox transmissions [26], gear trains, spur gears, and twisted string actuators (TSA) [27] can be used. Such micro-transmissions must overcome significant internal friction which commonly plague millimeter-scale mechanisms [28]. No existing solutions for ESD retraction can control the degree of tissue retraction, operate independently of endoscopes position or orientation, and remain minimally invasive by navigating through the endoscopic working channel to the surgical site.

This paper presents the first ESD retraction device that is wireless, decoupled from the endoscope, and able to provide adjustable control of tissue tension through the use of a unique magnetic micro-transmission called a magnetic twisted string actuator. The endoscopic magnetic retraction device (termed the twisted string actuator for retraction, or TSA-R) is seen in Fig. 1, and is 3.25 mm wide and 45 mm long. The device is compliant and small enough to pass through the working channel of a flexible endoscope at its minimum radius of curvature in a maximum retroflexion configuration. The TSA-R can generate 0.34 N of retraction force at a distance of 150 mm, 24 times stronger than a direct-pull magnetic anchor system of same the volume to the entire device. The ESD device can retract a distance of 20 mm in 105 turns at a contraction rate of 0.24 mm/s.

In this paper the device model-based design, characterization, mechanical validation, and clinical feasibility are presented. The theoretical models presented in Section III are validated experimentally to ensure agreement between theoretical and experimental results. These models are then used to guide the design dimensions of the TSA-R that meets the desired clinical constraints and criteria. The device must be able to pass through the flexible endoscope's working channel (diameter less than 3.7 mm) at its minimum radius of curvature (radius of 22.4 mm) in a retroflexion orientation (210°). The TSA-R must achieve a string contraction length of 20 mm, as the ESD technique targets lesions of a diameter of 20 mm or larger. To provide tunable retraction, the device must meet the force requirements of 0.9 to 3 N of retraction force. The TSA-R must work at an actuation depth of 110 mm to accommodate the sagittal abdominal half-depth of metabolically obese patients. Clinical criteria include the overall goal to remain minimally invasive, maximize string contraction length, and maximize retraction force. These design constraints and criteria are incorporated into the theoretical model to determine the proposed device design. The TSA-R is then characterized and mechanically validated ensuring it meets the desired constraints and criteria. The device performance is investigated to ensure it meets procedural requirements to prove clinical feasibility. The TSA-R is the smallest endoscopic magnetic retraction device that can generate enough force to retract tissue. It is expected that deployment of this retraction device in human cases will lower overall procedural time, increase dissection speed, improve R0 resection rates, lower the rate of local reoccurrence, lower the risk of muscle perforation, and increase the number of lesions typically treated with this technique by accommodating larger lesions in harder to reach locations when compared to the conventional ESD technique [12], [29], [30]. This device would greatly improve the adoption of the ESD technique for the endoscopic removal of early GI cancers and expand its future medical applications.

II. ESD Retraction Device Concept

The ESD retraction system is composed of two parts; the TSA-R and the external magnetic actuating unit which generated the magnetic field to drive the TSA-R. The device dimensions, components, and material decisions were informed by the presented model of device performance such that the device met the constraints and criteria mentioned in Section I. The assembled TSA-R, as seen in Fig. 1, is composed of a N50 neodymium iron boron (NdFeB) diametrically magnetized cylindrical internal permanent magnet (IPM) (Cyl0065D, SuperMagnetMan). This permanent magnet was chosen such that it was small enough to fit within the device and pass through the endoscopic working channel. A synthetic sapphire endstone jewel bearing (E2.49, Swiss Jewel Company) was used as a thrust bearing between the rotating magnet and the housing to reduce friction. Ultra-high molecular weight polyethylene (UHMWPE, Fiber-LINE) was chosen as the twisted string material. This fiber-based string was chosen due to its high Young's modulus, small string radius, and as reported in [27], reduces the string resisting torque, leads to a good modeling agreement with experimental testing, and gives repeatable results. Two aluminum repositionable clip anchor loops (McMaster-Carr) and a 3 mm brass chain (Hi Beads) were added to aid with device deployment. Finally the 3D-printed clear resin body (Form 3+, Formlabs) was designed such that it could pass through the working channel of the flexible endoscope. The material costs incurred to fabricate this single-use prototype was \$3.92 CAD.

The external actuation unit is composed of a 1.5 inch cubic N52 NdFeB permanent magnet (BX8X8X8, K & J Magnetics). This external permanent magnet was chosen using the magnetic modeling presented in Section III, such that it could generate a rotating magnetic field adequate to actuate the device at the abdominal depth of a metabolically obese patient is 110 mm and 100 mm for men and women, respectively [31]. The DYNAMIXEL robot actuator (XM430-W210-T) was chosen for its adequate stall torque and the desired frequency to actuate the external permanent magnet. The compatible Shield (DYNAMIXEL) and microcontroller (Arduino UNO) were selected. Finally, an optical board (Newport Optics) and extruded aluminum framing (McMaster-Carr) were constructed to house all components creating a surgical bench-top actuator for experimentation. The material costs incurred to fabricate this reusable prototype was \$509.93 CAD.

A. Procedural Implementation

The retraction device must be deployed and used in a series of steps to be implemented during an ESD procedure. Prior to device deployment the procedure itself can be performed under general anesthesia or conscious sedation, and is shown schematically in Fig. 2. Depending on the lesion's location within the GI tract, a flexible endoscope is advanced to the area through the mouth or anus without the need for any skin incisions. The lesion is carefully evaluated optically for its size and extent of lateral spread as well as any potential worrisome tissue features which could raise a concern for more advanced malignancy. The lesion edges are carefully marked using superficial cautery to ensure that clear margins can be achieved during the resection. Once this preparation is completed, the surgeon injects fluid (methyl blue saline) under the mucosal lesion to separate it from the deeper muscle layers of the GI wall. Using specialized electrocautery knives, the surgeon then incises the mucosa along the previously marked margin.

The TSA-R then travels through the flexible endoscope's working channel towards the surgical workspace as seen in Fig. 1. Once inserted into the field of view a repositionable clip is advanced through the working channel and is used to grab a looping anchor of the TSA-R. The repositionable clip is installed into the GI wall opposite the tissue of interest in the direction of desired retraction. A second repositionable clip is advanced into the surgical workspace anchoring the other loop of the TSA-R. The last repositionable clip is navigated to grasp the chain connected to the traction strings of the TSA-R and anchored to the lip of the circumferential incision, exposing the mucosal layer for dissection. Once installed, the external actuation unit is visually aligned outside the abdomen along the same axis of the IPM within the TSA-R, instantaneously coupling once the magnetic field is applied. The operator or surgical assistant controls the retraction of the TSA-R by controlling the rate and direction of rotation of the external actuation unit to provide optimal tissue tension

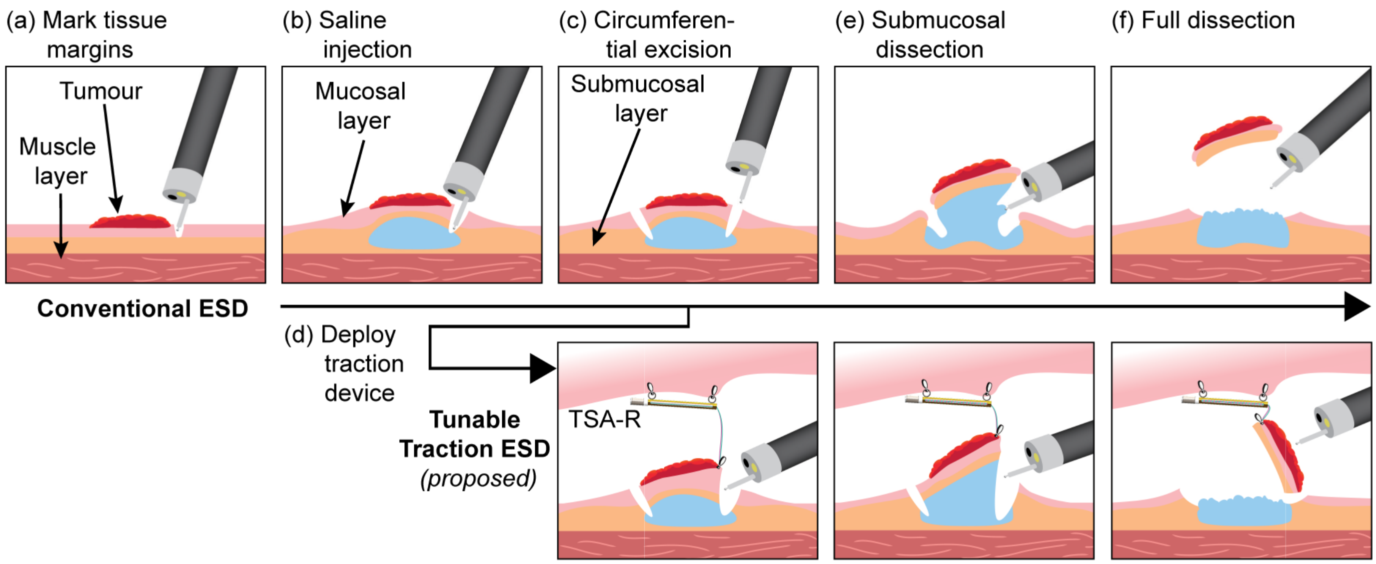

Fig. 2. Illustration comparing conventional and the proposed ESD procedure with TSA-R.

throughout the entirety of the procedure. During the dissection, the lesion is undermined and separated from the muscle. The procedure is complete when the lesion has been entirely divided from the surrounding mucosa circumferentially and fully separated from the GI muscle wall with a deep margin. The device is pulled out of the GI wall releasing the repositionable anchors and removed endoscopically as the flexible endoscope is withdrawn from the surgical workspace.

III. Device Mechanism Design

An overview of the device mechanism design incorporating the magnetic and TSA modeling is demonstrated in the schematics at different states as seen in Fig. 3. The theoretical models presented below aided in the device design parameters such that the TSA-R met all procedural ESD performance requirements.

A. Magnetic Modeling

To design the retraction device with the desired retraction force and string contraction length, magnetic torque and force analysis was conducted on the external permanent magnet to IPM interaction. This is standard magnetic modeling, stated here to provide background. The rotating magnetic field strength from a single permanent magnet was calculated using the dipole model shown in (1) [28].

$$\mathbf{B} = \frac{\mu_0}{4\pi}\frac{1}{\|\boldsymbol{p}\|^3}\left[3(\hat{\boldsymbol{p}}\cdot\hat{\boldsymbol{p}}^\top) - \mathbb{I}\right]\cdot\boldsymbol{m_2} \tag{1}$$

In this equation, $\boldsymbol{m_2}$ is the magnetic dipole moment of the actuating external permanent magnet, $\boldsymbol{p}$ is the position of the external permanent magnet dipole relative to the IPM of the device set to the origin at [0,0,0], and μ_0 is the vacuum permeability.

The input magnetic torque τ_m that drives the twisting of the strings is shown in (2). Where $\boldsymbol{m_1}$ is the magnetic dipole moment of the IPM, $\boldsymbol{B}$ is the magnetic field strength generated by the external permanent magnet, and γ is the angle between the dipole vector and the field vector. The magnetic torque is maximized when the field and dipole vector are perpendicular $\gamma = \pm 90°$, and zero when they are parallel at $\gamma = 0°$ and $180°$.

$$\tau_m = \|\boldsymbol{m_1}\|\|\boldsymbol{B}\|\sin(\gamma) \tag{2}$$

The magnetic dipole moment in (1) and (2) can be calculated using (3), where B_r is the residual flux density of the permanent magnet and V is the volume of magnetic material.

$$m_d = \frac{B_r V}{\mu_0} \tag{3}$$

The pull force between two magnetic dipoles along the Z-axis is seen in (4). Here, d is the distance from the center of the IPM to the center of the external permanent magnet along the Z-axis. This is used to determine the inter-magnetic forces and to compare the retraction device to an anchor-based direct magnetic retractor system.

$$F_z(d, m_1, m_2) = -\frac{3\mu_0 m_1 m_2}{2\pi d^4} \tag{4}$$

B. Twisted String Modeling

In this section, we investigate the basic principles of TSAs using standard modeling. These micro-transmissions are powerful, simple, lightweight, compact, and have a high transmission ratio where very low input torque can generate a large output force. The TSA model is a kineostatic model that assumes the twisting strings are rigid cylinders that are not compressible but easily deformable. The model presented below is adapted from [27], [32], [33] but repeated here for completeness.

There are two kinds of TSAs; linear slide or separator-type. Each type has a different kineostatic relationship that transmits rotational input into linear displacement and an axial force (retraction force).

The linear slide design consists of two strings fixed at either end. One side of the strings are connected to the IPM that provides rotational input to the actuator while the other is connected to a linear slide that is constrained by guides. The string contraction length (ΔL_2) achieved when IPM is rotated θ times is calculated using (5). Where L_0 is the twisting zone length, r_s is the radius of the string, and α is the twisting angle of the strings.

$$\Delta L_2 = L_0 - L_0\sec(\alpha) = L_0 - \sqrt{L_0^2 - r_s^2\theta^2} \tag{5}$$

The maximum stroke of the actuator is a geometric constraint based on the number of twists of the string achievable within a given twisting zone length such that the TSA does not over-twist. The over-twist region is defined as large strains that twist beyond the

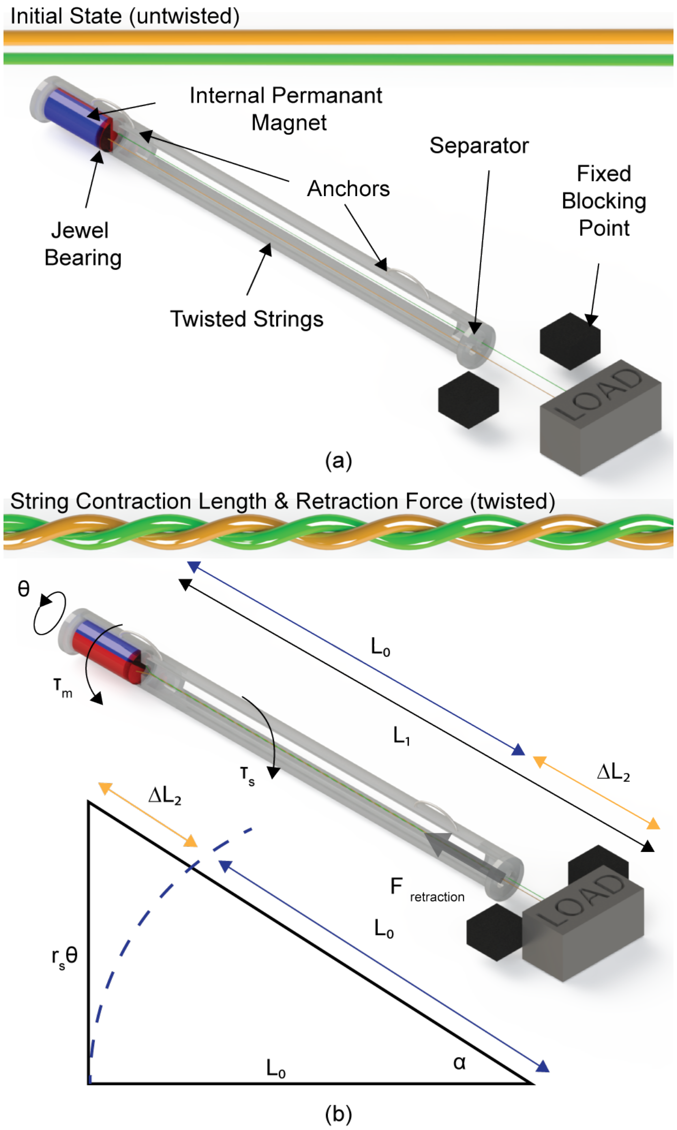

Fig. 3. The initial state (a) prior to actuation with an overview of the mechanism components, and the actuated state (b) demonstrating magnetic and TSA interaction, and the geometric relationship.

regular twisting stage, when the strings begin to non-uniformly and unpredictably knot and coil about themselves resulting in permanent plastic deformation and increased non-linearity, as seen in Fig. 5(a). While some researchers leverage this large strain using advanced modeling techniques or mechanisms [34], this study aims to keep actuation in the elastic region below the maximum stroke of the actuator. In (6) this is $\approx 0.36L_0$. The stroke of the actuator is determined primarily by the string radius (r_s) and length of twisting zone (L_0). The stroke of the actuator decreases as the length of the twisting zone decrease with each stroke as the string contracts. Conversely, the separator model has a fixed L_0. The ΔL_2 achievable under rotational input θ is given in (7). The maximum stroke of the actuator achievable in (8) is $\approx 0.58L_0$, this design can achieve a greater string contraction length due to its fixed twisting zone length. The twisting zone length does not decrease with each stroke of the actuator when compared to (6), making it the preferred design to maximize output retraction.

$$S_{max} = (1 - 2/\pi)L_0 \tag{6}$$

$$\Delta L_2 = L_0 \sec(\alpha) - L_0 = \sqrt{L_0^2 + r_s^2\theta^2} - L_0 \tag{7}$$

$$S_{max} = (\pi/2 - 1)L_0 \tag{8}$$

The transmission ratio of the separator design is derived in (9) below:

$$\frac{F}{\tau_m} = \frac{\mathrm{d}\theta}{\mathrm{d}\Delta L_2} = \frac{\sqrt{L_0^2 + r_s^2\theta^2}}{r_s^2\theta} \tag{9}$$

where F is the retraction force and τ_m is the input magnetic torque. The maximum retraction force of the actuator is dependent on the τ_s string resisting torque and the τ_m input magnetic torque as seen in Fig. 3. When retracting tissue the mechanism reaches the blocking point as illustrated in Fig. 3(b). As the strings continue to twist a string resisting torque (τ_s) builds as the individual string fibers uncoil. When τ_s becomes greater than τ_m the IPM slips, de-synchronizing with the rotation of the applied magnetic field ($\boldsymbol{B}$), causing a drop in retraction force, as seen in Fig. 9(b).

IV. Experiments

In this section, we validate the magnetic and TSA models presented above to characterize the performance of the system and guide the selection of design parameters to meet desired procedural metrics outlined in the introduction. To demonstrate the feasibility of this methodology and prove the device is able to repeatably control the degree of retraction during an ESD procedure, a clinical feasibility study is completed. Furthermore, the device is compared to previous solutions exhibiting its superior performance and novelty.

A. Characterization of TSA-R Device

A fixture was fabricated to actuate, measure, and isolate the mechanism in order to characterize the $F_{\text{retraction}}$ and ΔL_2 for the design of the TSA-R that met procedural requirements. The experimental apparatus used is seen in Fig. 4. The apparatus was designed to resemble a bench-top testing surgical platform. The external permanent magnet actuator was positioned beneath the hypothetical surgical workspace, such that the distance d between the external permanent magnet and IPM could replicate the desired abdominal depth within a patient.

1) String Contraction Length (ΔL_2): To validate the theoretical model presented in (7) and the repeatability of the system the ΔL_2 and S_{max} was measured over 5 trials at a set number of turns of the external permanent magnet until over-twist for different L_0. Initially, the ultra-high molecular weight polyethylene strings were pretreated in order to ensure agreement between experimental and theoretical results. The strings have the undesirable behaviour of elongating gradually under axial load due to the individual string bundle fibers rearranging as well as creep. The pretreating procedure consists of twisting and untwisting the strings a total of 100 turns at a frequency of 1 Hz, following the protocol from [27]. After pretreating, the string radius r_s was measured using scanning electron microscope (SEM). The r_s is an important value within the kineostatic model as the error is exponentially multiplied with each stroke of the actuator. Therefore, determining the exact radius is key to model agreement. For SEM imaging the string samples were gold sputtered to improve imaging quality. Next, multiple images (Fig. 5(d)) were taken visualizing the samples such that 12 measurements of the strings diameters could be recorded. The average string radius was 64 $\pm$ 6.5 μm. Fig. 5(c) compared a pair of pretreated and a single untreated ultra-high molecular weight polyethylene string. Due to preparation of

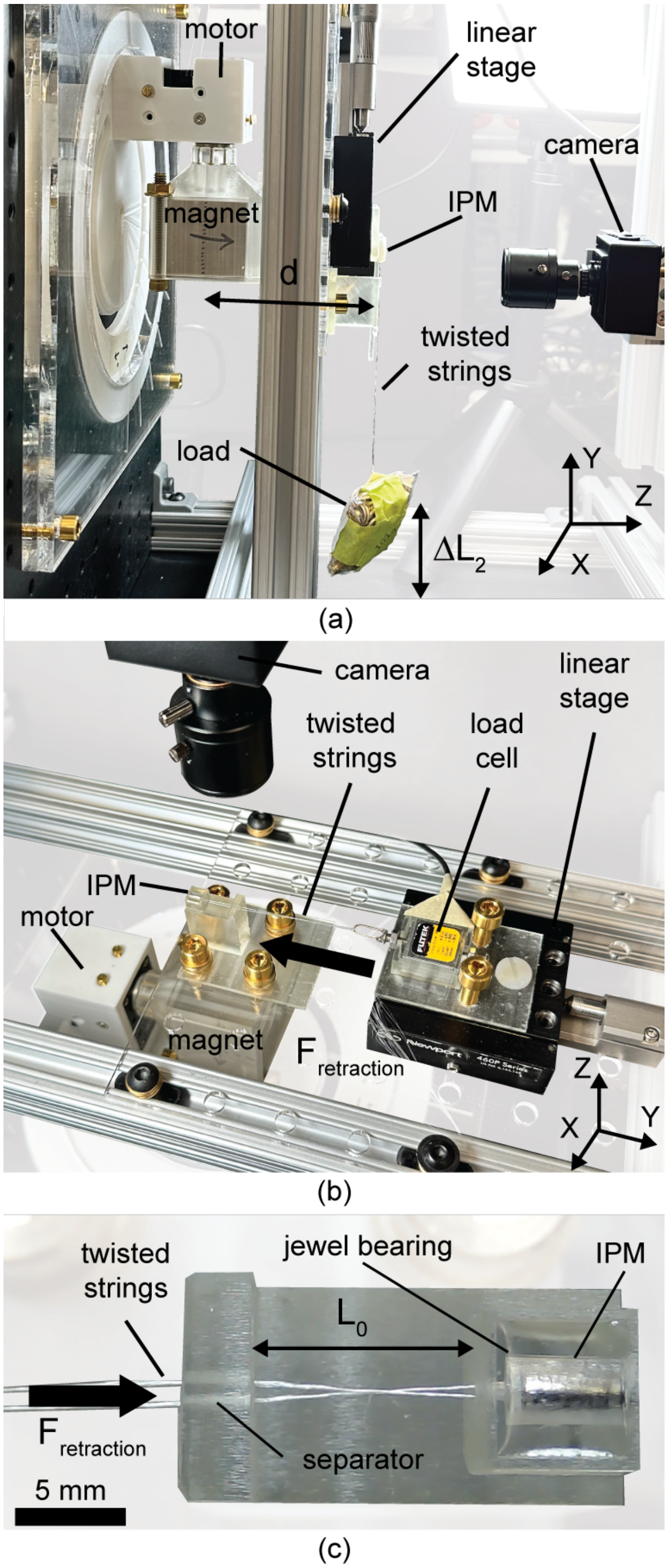

Fig. 4. Experimental apparatus used to characterize the TSA-R. (a) Apparatus configuration to measure $\boldsymbol{\Delta L_2}$. (b) Apparatus configuration for $\boldsymbol{F}_{\text{retraction}}$ testing. (c) Device mechanism components within the experimental apparatus.

the material the air gaps between the individual string fibers were removed resulting in a much smaller r_s.

To validate the model the ΔL_2 versus number of turns was measured when changing the L_0, the results are show in Fig. 5(a). As the L_0 is increased the the maximum ΔL_2 achievable also increased before S_{max}, however the rate of ΔL_2 decreases with an increase in L_0. This is due to the amount of turns required to remove air gaps between the pair of twisting strings.The model presented in (7) has good agreement to the experimental results and can therefore be used in the design of the TSA-R. As ESD is typically conducted on lesions with a diameter of 20 mm, the proposed TSA-R is required to retract 20 mm to provide tension throughout an entire dissection. A L_0 = 35 mm was chosen to achieve 20 mm of ΔL_2 before entering the over-twist zone, this was determined using S_{max}. The device was found to retract a distance of 20 mm in 105 turns without entering the over-twist zone at a speed of 0.2 mm/s. Next, the ΔL_2 under different constant loads (0.03 - 1 N) at a set L_0 = 10 mm over 5 trials was measured, the results are seen in Fig. 5(b). As the applied load increases, the maximum ΔL_2 decreases due to the increased load removing the air along the length of the string bundle fibers and contact friction. This causes the r_s to be smaller, decreasing the stroke of the actuator.

2) Retraction Force (F) and Twisting Zone Length (L_0): The effect of L_0 on F was investigated. The retraction force at a d = 120 mm was measured using a load cell (LSB200, Futek) rigidly connected to the twisted strings with an adapter while changing L_0. The experimental apparatus used is presented in Fig. 4(b), and the results are plotted in Fig. 6. Each trial was actuated past IPM slip, causing subsequent collection and slips. Permanent magnet slip is the point when the $\tau_m \leq \tau_s$, causing the the IPM to de-synchronize with the rotating magnetic field ($\boldsymbol{B}$) generated by the external permanent magnet. This point is typically when the retraction force peaks for a given τ_m.

The number of turns required to reach the peak retraction force increases with an increase in L_0. This is due to the number of pre-turns required prior to active turns. Pre-turns are the turns when the string slack is collected as seen in Fig. 3(b). Once all the slack along the length of the strings is collected a blocking point is reached (Fig. 3(b)). At the blocking point ΔL_2 does not increase but the strings continue to twist generating an axial force along the length of the fibers. This continues until the $\tau_m \leq \tau_s$ when IPM slip occurs, as seen in Fig. 6. The twisting and untwisting about the peak retraction force is due to the de-synchronization of the IPM to the rotating magnetic field ($\boldsymbol{B}$).

3) Retraction Force - Hysteresis and Stress Relaxation: While the model used in this study is kineostatic we investigate the viscoelastic properties of the ultra-high molecular weight polyethylene material to characterize its effect. The experimental apparatus in Fig. 4(b) was used with a d = 100 mm, L_0 = 35 mm, and the twisted strings were rigidly connected to the load cell. The retraction force was measured while twisting and untwisting the IPM a set number of turns as seen in Supplementary Fig. 1(a). Three different L_0 were tested over 3 trials at a different number of pre-twists. For each trial a total of 20 turns were completed while the number of pre-twists and active twists were varied. It was found that the material demonstrated viscoelastic properties due to loading and unloading loops not following the same trajectory. The rate at which the axial force is generated during loading is less than the rate it is lost during unloading, meaning the mechanism loses energy during untwisting. Comparing the number of pre-twists, the rate of retraction force is higher as more turns are active than passive towards force generation.

Stress relaxation was examined by collecting the retraction force over 5 trials at a d = 100 mm with a L_0 = 40 mm using a load cell rigidly connected to the twisting strings as seen in Fig. 4(b). The strings were twisted exactly 12 turns using the external permanent magnet to a peak force of 0.58 ± 0.05 N. The external permanent

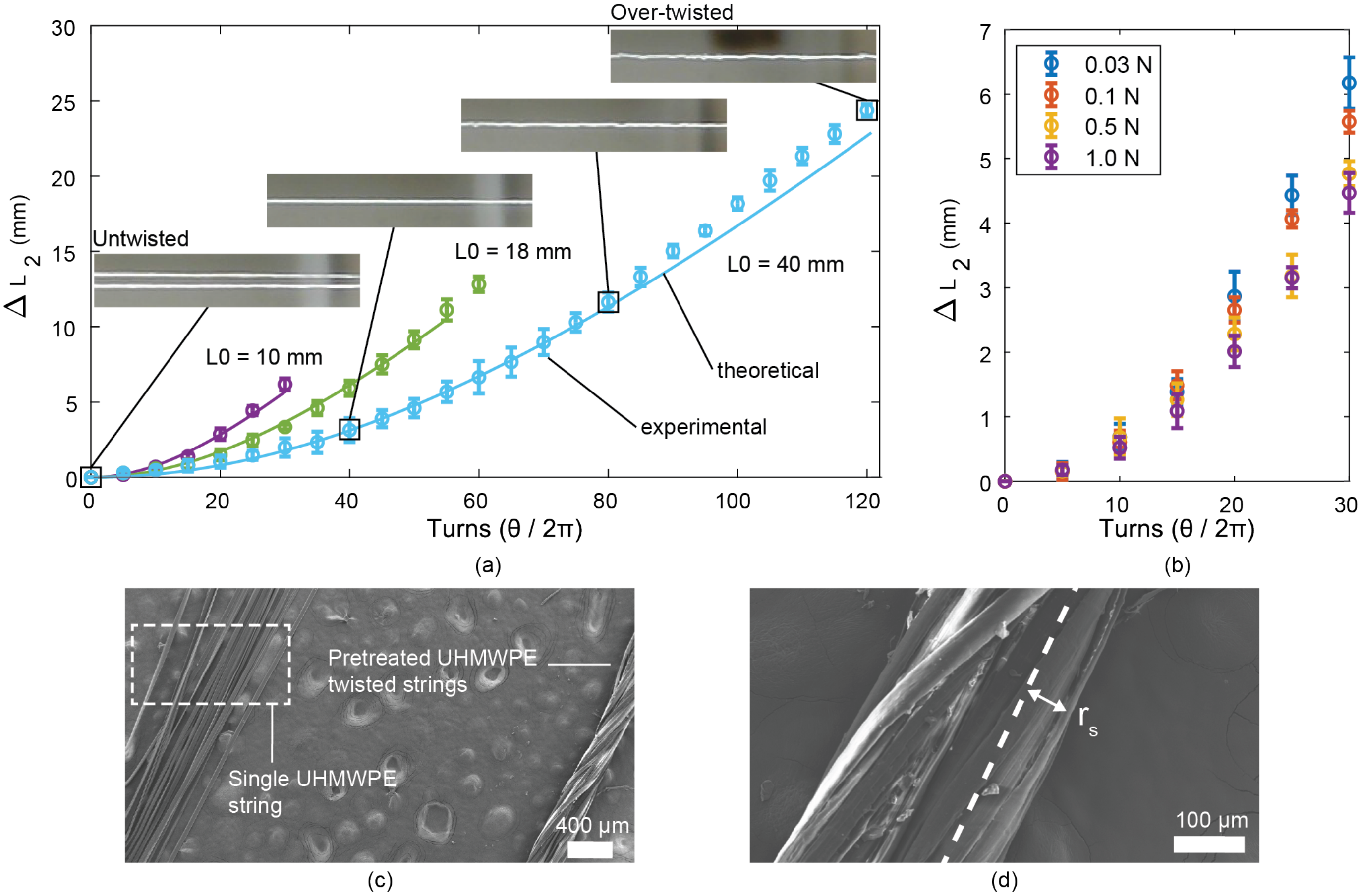

Fig. 5. (a) Comparison of ΔL_2 vs turns at d = 100 mm with twisting string stills showcasing the different states of twisting until over-twist (n = 5, error bars are standard deviation). (b) ΔL_2 vs turns with L_0 = 10 mm when a load is applied (n = 5, error bars are standard deviation). (c) SEM image comparing untreated and pretreated ultra-high molecular weight polyethylene strings. (d) SEM image used to measure r_s.

magnet was held in the same rotational position for 5 mins and the final retraction force was measured to be 0.36 ± 0.01 N. Due to stress relaxation over the 5 mins period a 38.6% drop in retraction force was experienced, as seen in Supplementary Fig. 1(b).

4) Working Channel Minimum Radius of Curvature: The ability of the TSA-R to deform and bend was tested to ensure it could travel through the working channel of a flexible endoscope to the surgical workspace during a procedure. GI flexible endoscopes have a working channel diameter of 3.7 mm and are able to achieve a variety of configurations in order to navigate the tortuous path of the GI tract. In a retroflexion configuration it can bend 210 °, the most extreme bending a flexible endoscope could achieve, with a minimum radius of curvature of 22.4 mm. An apparatus modeled after the most extreme parameters (working channel, radius of curvature, and degree of flexion) of the GI scope was 3D-printed a seen in Fig. 7. The fully assembled TSA-R was successfully pushed through the entirety of the mock working channel with no permanent damage or deformation.

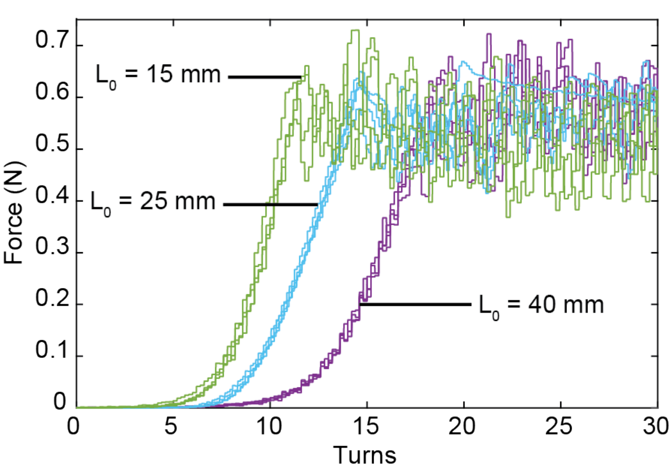

Fig. 6. Retraction force vs turns comparing different L_0 at d = 120 mm (n = 4 for each L_0)

B. External Actuation Unit Characterization

1) Verification of Magnetic Modeling: A fixture was fabricated to confirm that the dipole magnetic model was accurate when predicting $\boldsymbol{B}$, for control of the device via the external actuation unit, as seen in Supplementary Fig. 2. The fixture held a 1-axis transverse gaussmeter probe (Gaussmeter 425, LakeShore) perpendicular to the external permanent magnet such that the probe's active area was centered to the magnetic dipole moment of the external permanent magnet. The probe was repeatedly advanced from 250 mm to 1.5 times the radius of the external permanent magnet, with the field strength measured incrementally. The minimum distance of 1.5 times the normalized distance from the center of the external permanent magnet to the gaussmeter probe was chosen as the optimal distance for the dipole field approximation as its error is less than 1 % [35]. The probe was held at each distance for 1 minute to ensure the field reading had settled and an average of 5 measurements were

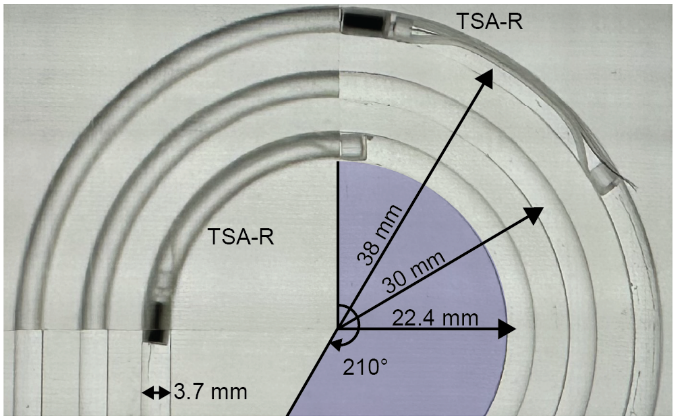

Fig. 7. Devices passing through a clear 3D-printed endoscope working channel phantom.

taken. The results comparing the dipole model approximation and experimental results are plotted in Fig. 8(a).

2) Retraction Force at a Distance (d): The retraction force at a distance (d) between the centers of the external permanent magnet and IPM were measured using a load cell rigidly connected to the twisting strings while the mechanism was rigidly fixed, as seen in Fig. 4(b). The d was incrementally increased from 55 mm to 200 mm with a fixed L_0 = 35 mm while the external permanent magnet was rotated 60 times, the results are demonstrated in Fig. 9. As the d between the external permanent magnet and IPM decreases the peak retraction force increases, this is due to the increased τ_m caused by an increase in $\boldsymbol{B}$. This increases the point of slip as the τ_m can overcome τ_s, achieving a greater number of turns and subsequently a higher retraction force. Fig. 9(c) shows the relationship between retraction force and distance. This plot is the average retraction force of the first 4 peaks for each trial versus the distance between the magnet centers, as seen in Fig. 9(a).

3) Performance Due to Misalignment of external permanent magnet to IPM: This section theoretically investigated the impact

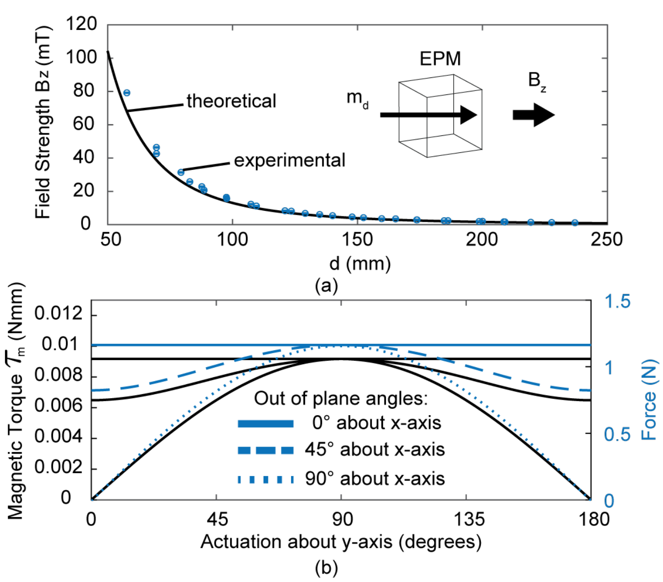

Fig. 8. (a) Magnetic field strength ($\boldsymbol{B_z}$) vs distance from a single cubic permanent magnet (38.1 mm x 38.1 mm x 38.1 mm) modeled as a dipole (n = 5, error bars are standard deviation). (b) Input magnetic torque (τ_m) vs rotation about y-axis at different misalignments about the x-axis. The resultant output retraction force due to a decrease in τ_m.

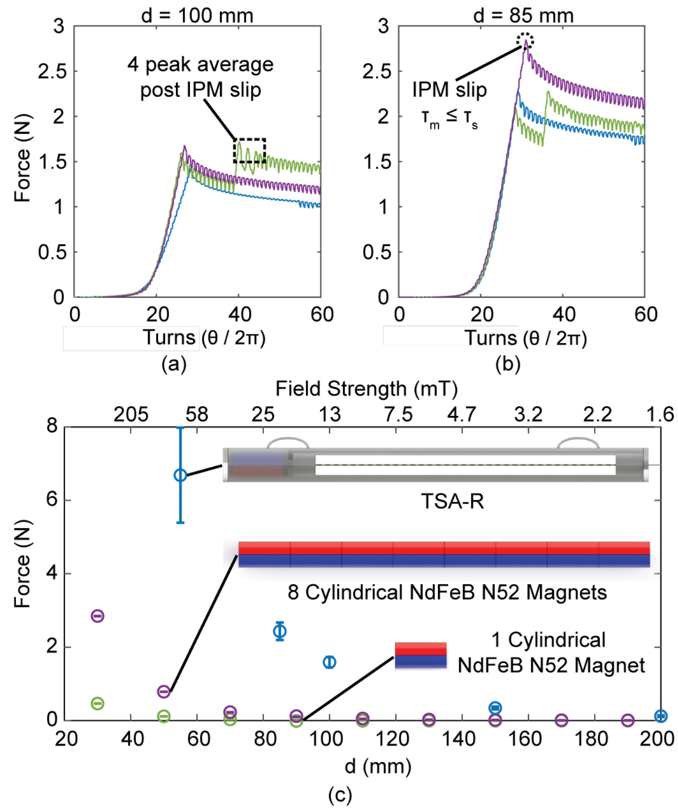

Fig. 9. Retraction force vs turns at $\boldsymbol{L_0}$ = 35 mm and frequency of 1 Hz for (a) $\boldsymbol{d}$ = 100 mm and (b) $\boldsymbol{d}$ = 85 mm. (c) four-peak average device retraction force versus distance ($\boldsymbol{d}$) and field strength ($\boldsymbol{B}$) (n = 3, error bars are standard deviation), compared to magnetic anchor systems with 1 and 8, 2.5 mm wide by 5 mm long cylindrical magnets (n = 5, error bars are standard deviation).

of misalignment of the magnetic dipoles of the external permanent magnet and IPM. Since the GI tract is deep within the abdominal cavity visualization is limited to the camera on the endoscope. Fig. 8(b) displays the effect of out-of-plane rotation (the angle between the two magnetic dipoles) on the output retraction force. Misalignment causes a decrease in magnetic torque as seen in (2) until complete failure when the magnetic dipoles are parallel. The output retraction force achievable based off of these input torques was calculated using the experimental data from Fig. 9 and (1), where the τ_m was interpolated based on the distance between dipoles. The theoretical τ_m due to misalignment was calculated and converted to the retraction force using the relationship in Fig. 9(c).

C. Device Performance

1) Retraction Force of Magnetic Anchor versus TSA-R: The TSA-R was compared to the magnetic anchor systems to examine their degrees of retraction force. The magnetic anchor retraction devices as introduced in Section I, work by coupling a small permanent magnet clipped to the tissue of interest with a larger external permanent magnet or electromagnetic navigation system. To compare the magnetic pull force (retraction) two magnetic anchor systems were created, as seen in Supplementary Fig. 3. One system has the exact same amount of magnetic material to the IPM used in the TSA-R, while the second system was composed of 8 times the amount of magnetic material, as if the entirety of the TSA-R volume was filled with magnetic material. The permanent magnets were mounted on a linear slide rigidly fixed to a load cell. The load cell and permanent magnets on the linear slide were centered to the external permanent magnet. The attractive pull force between the external permanent magnet and IPM was measured at incremental distances (d). The experimental results are plotted in Fig. 9(c). At a d = 150 mm the TSA-R could generate a retraction force of 0.34 N, 24 times greater than the magnetic anchor with the maximum amount of magnetic material, and 163 times stronger than a magnetic anchor of the same volume to the IPM in the TSA-R. The magnetic anchor systems could only generate significant retraction forces at a $d \leq 50$ mm, this is insufficient as the radius of the external permanent magnet is 27 mm and IPM is 1.25 mm leaving 21.75 mm of abdominal wall thickness and GI depth to sufficiently couple to the external permanent magnet. This is problematic as the sagittal abdominal half-depth of metabolically obese men and women are 110 mm and 100 mm, respectively [31].

2) Clinical Feasibility: An ex-vivo experimental ESD procedure was completed to prove clinical feasibility regarding the deployment, use, and removal of the TSA-R. The experiment was conducted by an experienced GI endoscopist completing a mock ESD procedure on a gastric phantom as seen in Fig. 10(a). The gastric porcine model came from an animal that was greater than 30 kgs and was received frozen having been stored at -16°C. The organ was thawed in saline for 12 hours prior to the procedure. The animal model was initially cleaned with lukewarm water and dish soap, then mounted into the experimental apparatus as seen in Fig. 10(a). The lesser curvature of the stomach was sutured shut to allow for insufflation during the procedure (Fig. 10(a)). An overtube was sealed to an opening of the stomach using plastic clamps, simulating an esophagus and marking the entry point for the flexible colonscope (colonovideoscope CF type H180AL, Olympus). During insufflation the distance d between the IPM and external permanent magnet varied between 60 to 120 mm, as seen in Fig. 10(b).

The clinician then completed an ESD procedure on the animal model using the TSA-R, targeting the gastric body following the procedure outlined in Fig. 2. Initially the device was deployed endoscopically using repositionable clips (Fig. 10(f)i). The surgeon then injected saline into the submucosal layer of the GI wall lifting the mucosa off of the gastric muscle wall (Fig. 10(f)ii). An electrocautery knife (HookKnife, Olympus) was used to complete a circumferential incision prior to traction being applied (Fig. 10(f)iii). The TSA-R was magnetically actuated using the external permanent magnet as seen in Fig. 10(b), this caused the TSA-R's strings to contract in length. The device was able to provide tunable traction, exposing the dissection plane, and ensure no gastric muscle perforation (Fig. 10(f)iv). Dissection continued through the submucosal layer (Fig. 10(f)v.) until the entire lesion was excised (Fig. 10(f)vi.) such that the procedure was complete and the whole device could be removed from the surgical workspace. Device removal was achieved by grasping the TSA-R with a single-use repositionable clip and pulling to release the device from the mucosal wall. Once securely grasped the TSA-R with attached lesion of interest were removed from the surgical workspace as the colonscope is withdrawn from the entry point. The device post-procedure was examined and no permanent damage was noticed, however it was covered in gastric fluids (Fig. 10(d)). The entire procedure was recorded and can be seen in Supplementary Video 1. The procedural time for deployment, dissection, and removal were recorded, the entire procedure from insertion to removal took 30 minutes. The lesion was mounted post excision (Fig. 10(e)) and had a surface area of 67 mm^2. The average dissection speed was recorded at 11.3 cm^2/hour, this is 1.25 times faster than the international benchmark of 9 cm^2/hour [36]. Unedited original images of the endoscopic view can be found in Supplementary Fig. 4.

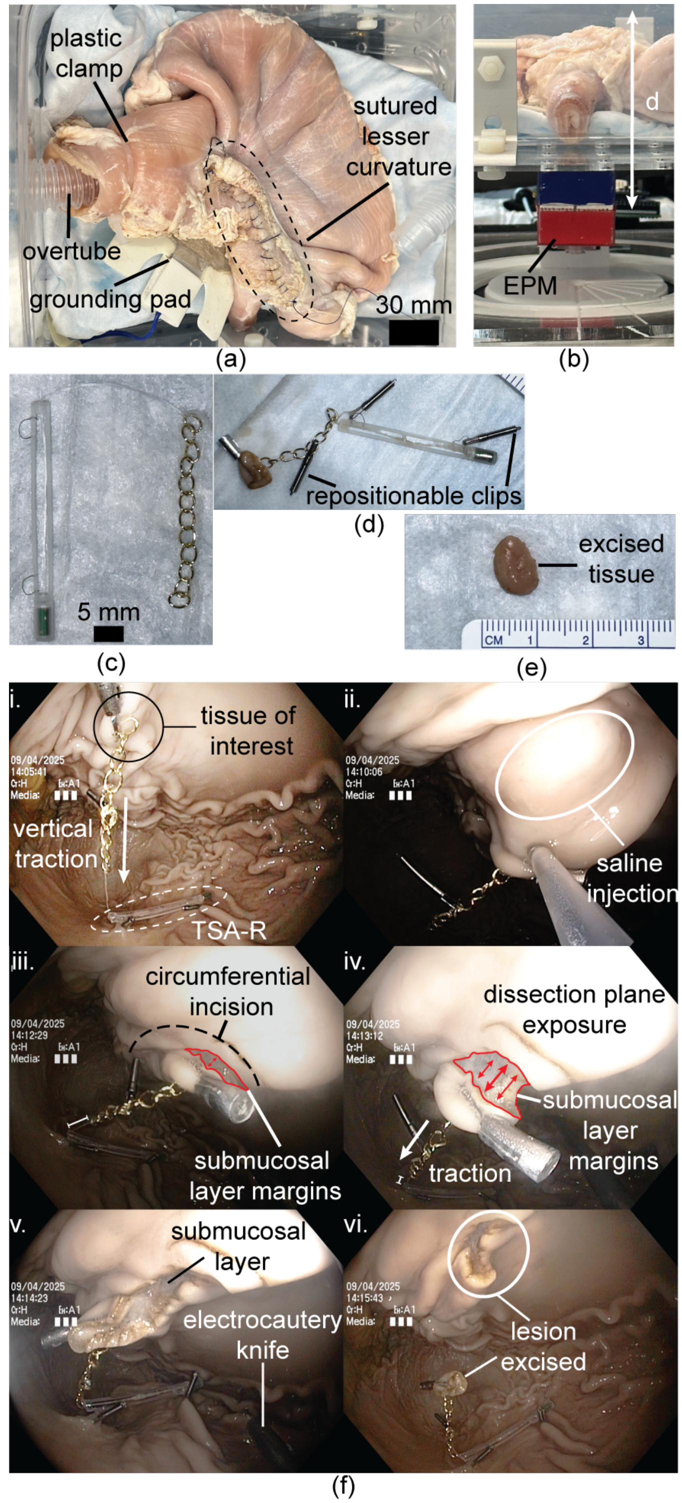

Fig. 10. (a) Top view of experimental apparatus for ex-vivo testing. (b) Side view of experimental apparatus. (c) TSA-R pre-procedure. (d) TSA-R post ex-vivo ESD procedure. (e) Excised lesion from procedure. (f) Endoscopic stills (images enhanced by lightened shadows, reduced exposure, and increased brightness) of ESD procedure demonstrating i. device deployment, ii. saline injection, iii. circumferential excision before traction is applied, iv. traction applied via magnetic actuation of the TSA-R exposing the dissection plane, v. dissection through the submucosal layer with HookKnife, and vi. full dissection of the entire lesion from gastric wall.

V. Discussion and Future Work

The final design parameters for the TSA-R were initially driven by theoretical modeling of the mechanism and confirmed with experimental results. The amount of ΔL_2 achievable is dependent on the length of the twisting zone (L_0) and stroke of the actuator (r_s). It can achieve a maximum string contraction length of 20 mm before entering the over-twist zone. Most pre-cancerous lesions selected for ESD procedures have a diameter greater than 20 mm. Therefore, retracting a distance of 20 mm is sufficient, but more retraction is always desired. The diameter of the GI tract ranges from 10 to 100 mm, limiting the allowable device length. Future work will focus on increasing string contraction and reducing the device's aspect ratio by leveraging the 8 independent control outputs or the kinematic constraints of magnetic actuation by utilizing the external actuation unit's single input field direction as seen in [37].

The TSA-R peak retraction force is dependent on the τ_m, however at a minimum distance of 55 mm a peak retraction force of 7.98 N; four-peak average of 5.62 N was achieved. This is sufficient as retraction force requirements have been reported between 0.9-3 N [38]. Increasing the retraction force is not required but increasing the actuation range of the TSA-R could be desirable. While this design can accommodate the average obese patient sagittal abdominal depth, cases that require greater range would require even greater B or m_d. This could be achieved by increasing the volume of the IPM or external permanent magnet. Changes to the IPM would reduce the ability of the device to be endoscopically delivered, while increasing the strength of the external actuation unit is possible. External actuation systems composed of permanent magnets or electromagnetic coils must increase in size and energy requirements in order to generate larger magnetic fields.

An improved force model is needed to account for TSA force output and the effects of string friction. Incorporating both inter fiber and at the separator friction, may explain variations in retraction force (Fig. 9) and potential IPM slip leading to undesirable premature untwisting. An improved model would allow for better control allowing the operator to set and maintain a desired force output, mitigating time-dependent viscoelastic behaviors, as shown by hysteresis and stress relaxation (Supplementary Fig. 1(a–b)).

A potential limitation of this work is the implementation of a magnetically actuated device within an operating room. Like all electrical equipment, it is possible that the field generation unit could interfere with sensitive medical equipment. However, the 10-90 mT magnetic field itself is only generated at low frequencies up to a few cycles per second and itself will not induce any noticeable currents in electrical equipment. During the experiments we ran for this work, we never observed interference with the flexible endoscope at the distal end within the surgical workspace. A magnetically actuated device like this in clinical use would however likely be contraindicated for patients with pacemakers or other implanted electronic devices out of an abundance of caution. Some caution is required when using a large external permanent magnet as it can become strongly attracted to any ferromagnetic materials within the environment such as a metal bed frame. It should be noted however, that the level of caution required would be much less than for example an MRI (which generate fields over an order of magnitude higher).

Other limitations in this work are the ability of the operator to align the external permanent magnet with the IPM to ensure proper actuation control. From Fig. 8(b), slight misalignment affects the output retraction force of the device. Aligning dipole vectors using only endoscopic imaging relies heavily on the skill of the endoscopist, their understanding of magnetic actuation, and can prolong procedures, potentially affecting clinical outcomes. Future work will involve incorporating an array of hall effect sensors to a more mobile external actuation unit like a handheld magnetic field generator such that their relative orientations can be easily triangulated, eliminating the need for visual alignment endoscopically and promoting faster deployment and actuation.

Finally, device deployment and installation is an additional procedural step not presently required in the conventional ESD procedure. The device is currently anchored within the GI tract using repositionable clips, a tool already deployed by endoscopists. As seen in Supplementary Video 1, the repositionable clips are ferromagnetic. This causes a swinging motion which could lead to premature failure or slip of the retraction device. While deployment and installation of repositionable clips are used in the partially adopted practice of clip-and-thread traction (or some variation) of this approach. Conventional ESD does not require the deployment of these clips, potentially resulting in longer procedural times. While this is potentially a limitation to the current device. Future work could investigate designing a unique anchoring system that does not require additional steps or devices to be inserted through the working channel. The impact of improved traction control should also be investigated as the trade off for increased procedural times. As the additional installation time might be mitigated by the improved control throughout dissection. This could result in less detrimental clinical outcomes and lowering the learning curve for novice endoscopists.

VI. Conclusion

This work presents the first wireless, flexible endoscope-decoupled ESD retraction device with adjustable tissue tension control, addressing key limitations in current conventional ESD tools. The TSA-R system leverages a micro-transmission TSA to achieve high force output while maintaining a compact form factor that allows delivery to the surgical workspace through a standard working channel of a colonovideoscope. Magnetic actuation enables the device to operate independently of the flexible endoscope, allowing the surgeon to maintain constant visualization of the dissection plane. Additionally, retraction performance is unaffected by the orientation or maneuverability of the flexible endoscope.

Ex-vivo evaluation using a porcine gastric model demonstrated the clinical feasibility of the TSA-R, achieving a dissection speed 1.25 times faster than the international benchmark, highlighting its potential to enhance ESD efficiency and safety. By enabling effective, wireless tissue retraction at clinically relevant abdominal depths, this device could support broader adoption of ESD for early GI cancer treatment.

Beyond ESD, the TSA-R platform may be adapted for a range of minimally invasive procedures that require high force generation and string contraction length in wireless, spatially constrained environments. A potential application includes organ retraction in abdominal laparoscopic surgeries. Overall, this work demonstrates a promising advance in the field of magnetic actuation and endoscopic tool design, with significant implications for both current ESD clinical practice and future surgical innovations.

Acknowledgment

Special thanks to Fibertech for lending the flexible endoscope for the ex-vivo experiments.

References

[1] Y. Xie *et al.*, "Gastrointestinal cancers in china, the usa, and europe," *Gastroenterology report*, vol. 9, no. 2, pp. 91–104, 2021.

[2] J. Tracht, B.S. Robinson, and A.M. Krasinskas, "Pathology of premalignant and malignant disease of the esophagus," *Esophageal Cancer: Prevention, Diagnosis and Therapy*, pp. 61–81, 2020.

[3] M.P. Kumarasinghe *et al.*, "Pathological assessment of endoscopic resections of the gastrointestinal tract: a comprehensive clinicopathologic review," *Modern Pathology*, vol. 33, no. 6, pp. 986–1006, 2020.

[4] T. Gotoda *et al.*, "Prospective clinical trial of magnetic-anchor–guided endoscopic submucosal dissection for large early gastric cancer," *Gastrointestinal Endoscopy*, vol. 69, no. 1, pp. 10–15, 2009.

[5] Y.M. Park *et al.*, "The effectiveness and safety of endoscopic submucosal dissection compared with endoscopic mucosal resection for early gastric cancer: a systematic review and metaanalysis," *Surgical Endoscopy*, vol. 25, no. 8, pp. 2666–2677, 2011.

[6] J.H. Yeh *et al.*, "Long-term outcomes of primary endoscopic resection vs surgery for t1 colorectal cancer: a systematic review and meta-analysis," *Clinical Gastroenterology and Hepatology*, vol. 18, no. 12, pp. 2813–2823, 2020.

[7] A. Fujimori *et al.*, "Pocket creation and ring-thread traction facilitates colorectal endoscopic submucosal dissection for non-experts," *in vivo*, vol. 35, no. 3, pp. 1655–1660, 2021.

[8] H. Ono *et al.*, "Guidelines for endoscopic submucosal dissection and endoscopic mucosal resection for early gastric cancer," *Digestive Endoscopy*, vol. 33, no. 1, pp. 4–20, 2021.

[9] S. Tanaka *et al.*, "Jges guidelines for colorectal endoscopic submucosal dissection/endoscopic mucosal resection," *Digestive Endoscopy*, vol. 27, no. 4, pp. 417–434, 2015.

[10] Q. Zhang, J.Q. Cai, and Z. Wang, "Usefulness of tumor traction with a snare and endoclips in gastric submucosal tumor resection: a propensity-score-matching analysis," *Gastroenterology Report*, vol. 9, no. 2, pp. 125–132, 2021.

[11] S. Suzuki *et al.*, "Usefulness of a traction method using dental floss and a hemoclip for gastric endoscopic submucosal dissection: a propensity score matching analysis," *Gastrointestinal Endoscopy*, vol. 83, no. 2, pp. 337–346, 2016.

[12] C. Lopimpisuth *et al.*, "Traction-assisted endoscopic submucosal dissection reduces procedure time and risk of serious adverse events: a systematic review and meta-analysis," *Surgical endoscopy*, vol. 36, no. 3, pp. 1775–1788, 2022.

[13] T.R. McCarty and H. Aihara, "Current state of education and training for endoscopic submucosal dissection: Translating strategy and success to the usa," *Digestive Endoscopy*, vol. 32, no. 6, pp. 851–860, 2020.

[14] M. Ryou and C. Thompson, "Magnetic retraction in natural-orifice transluminal endoscopic surgery (notes): addressing the problem of traction and countertraction," *Endoscopy*, vol. 41, no. 02, pp. 143–148, 2009.

[15] S.P. Aslam *et al.*, "Feasibility and safety of using a novel traction wire for endoscopic submucosal dissection of challenging gastrointestinal neoplasia," *Endoscopy*, vol. 54, no. 11, pp. E606–E607, 2022.

[16] H. Kaku *et al.*, "Endoscopic submucosal dissection using endotrac, a novel traction device," *Digestion*, vol. 102, no. 5, pp. 714–721, 2021.

[17] S. Abe *et al.*, "Efficacy of current traction techniques for endoscopic submucosal dissection," *Gut and liver*, vol. 14, no. 6, p. 673, 2020.

[18] H. Gao *et al.*, "Transendoscopic flexible parallel continuum robotic mechanism for bimanual endoscopic submucosal dissection," *The International Journal of Robotics Research*, vol. 43, no. 3, pp. 281–304, 2024.

[19] D.T.H. de Moura *et al.*, "Robot-assisted endoscopic submucosal dissection versus conventional esd for colorectal lesions: outcomes of a randomized pilot study in endoscopists without prior esd experience," *Gastrointestinal endoscopy*, vol. 90, no. 2, pp. 290–298, 2019.

[20] S.J. Phee *et al.*, "Robot-assisted endoscopic submucosal dissection is effective in treating patients with early-stage gastric neoplasia," *Clinical Gastroenterology and Hepatology*, vol. 10, no. 10, pp. 1117–1121, 2012.

[21] L. Zorn *et al.*, "A novel telemanipulated robotic assistant for surgical endoscopy: preclinical application to esd," *IEEE Transactions on Biomedical Engineering*, vol. 65, no. 4, pp. 797–808, 2017.

[22] L. Sliker *et al.*, "Magnetically driven medical devices: a review," *Expert review of medical devices*, vol. 12, no. 6, pp. 737–752, 2015.

[23] M. Mortagy *et al.*, "Magnetic anchor guidance for endoscopic submucosal dissection and other endoscopic procedures," *World Journal of Gastroenterology*, vol. 23, no. 16, p. 2883, 2017.

[24] N. Garbin *et al.*, "Laparoscopic tissue retractor based on local magnetic actuation," *Journal of Medical Devices*, vol. 9, no. 1, p. 011005, 2015.

[25] H. Sugerman *et al.*, "Intra-abdominal pressure, sagittal abdominal diameter and obesity comorbidity," *Journal of internal medicine*, vol. 241, no. 1, pp. 71–79, 1997.

[26] C. Hong *et al.*, "Magnetically actuated gearbox for the wireless control of millimeter-scale robots," *Science robotics*, vol. 7, no. 69, p. eabo4401, 2022.

[27] M. Nica, C. Forbrigger, and E. Diller, "A novel magnetic transmission for powerful miniature surgical robots," *IEEE/ASME Transactions on Mechatronics*, vol. 27, no. 6, pp. 5541–5550, 2022.

[28] J.J. Abbott, E. Diller, and A.J. Petruska, "Magnetic methods in robotics," *Annual Review of Control, Robotics, and Autonomous Systems*, vol. 3, no. 1, pp. 57–90, 2020.

[29] M. Yoshida *et al.*, "Conventional versus traction-assisted endoscopic submucosal dissection for gastric neoplasms: a multicenter, randomized controlled trial (with video)," *Gastrointestinal Endoscopy*, vol. 87, no. 5, pp. 1231–1240, 2018.

[30] ——, "Conventional versus traction-assisted endoscopic submucosal dissection for large esophageal cancers: a multicenter, randomized controlled trial (with video)," *Gastrointestinal endoscopy*, vol. 91, no. 1, pp. 55–65, 2020.

[31] U. Risérus *et al.*, "Sagittal abdominal diameter as a screening tool in clinical research: cutoffs for cardiometabolic risk," *Journal of obesity*, vol. 2010, no. 1, p. 757939, 2010.

[32] G. Palli *et al.*, "Modeling and control of the twisted string actuation system," *IEEE/ASME Transactions on Mechatronics*, vol. 18, no. 2, pp. 664–673, 2012.

[33] S. Jeong, Y. Lee, and K.S. Kim, "Applications: Twisted string actuation-based compact automatic transmission," in *2021 IEEE International Conference on Robotics and Automation*. IEEE, 2021, pp. 10 870–10 876.

[34] R. Konda, D. Bombara, and J. Zhang, "Overtwisting and coiling highly enhance strain generation of twisted string actuators," *Soft Robotics*, vol. 10, no. 4, pp. 760–769, 2023.

[35] A.J. Petruska and J.J. Abbott, "Optimal permanent-magnet geometries for dipole field approximation," *IEEE transactions on magnetics*, vol. 49, no. 2, pp. 811–819, 2012.

[36] T. Fox *et al.*, "Untutored learning curve for endoscopic submucosal dissection in new zealand," *New Zealand Medical Journal*, p. 55, 2022.

[37] H. Mayer *et al.*, "A compact dual-mode twisting retraction device for endoscopic submucosal dissection," in *2025 IEEE/RSJ International Conference on Intelligent Robots and Systems (IROS)*, 2025, pp. 21 410–21 416.

[38] D.Y. Shin *et al.*, "Compatibility of endoclips in the gastrointestinal tract with magnetic resonance imaging," *Scientific Reports*, vol. 10, no. 1, p. 16537, 2020.